Ph.D. Dissertation of Medicine

Recombinant Human Parathyroid Hormone-Soaked Nanofiber Sheet Accelerates Tendon-to-Bone Healing in a Rabbit Model of a Chronic Rotator Cuff Tear

토끼의 만성 회전근 개 파열 모델에서 나노섬유를 이용한 재조합 부갑상선 호르몬 담지 종이형 지지체가 회전근 개 건의 재생을 촉진시킨다

August 2022

Graduate School of Medicine
Seoul National University
Orthopedics Major

Jian HAN

Recombinant Human Parathyroid Hormone-Soaked Nanofiber Sheet Accelerates Tendon-to-Bone Healing in a Rabbit Model of a Chronic Rotator Cuff Tear

지도교수 오 주 한

이 논문을 의학박사 학위논문으로 제출함

2022년 4월

서울대학교 대학원
의학과 정형외과학
Jian HAN

Jian HAN의 박사 학위논문을 인준함
2022년 7월

Chair	김 한 수	(Seal)
Vice Chair	오 주 한	(Seal)
Examiner	임 재 영	(Seal)
Examiner	김 세 훈	(Seal)
Examiner	신 상 진	(Seal)

Abstract

Recombinant Human Parathyroid Hormone-Soaked Nanofiber Sheet Accelerates Tendon-to-Bone Healing in a Rabbit Model of a Chronic Rotator Cuff Tear

Jian HAN

College of Medicine, Orthopaedics Major

The Graduate School

Seoul National University

Introduction: Rotator cuff tears (RCTs) are a common and progressive disease of the upper extremity that causes pain and disorders of the shoulder joint. However, despite improvements in surgical techniques, postoperative healing failure remains a frequent complication, with the failure rates ranging from 11% to 94%. Osteoporosis is an independent prognostic factor for rotator cuff healing. Recombinant human parathyroid hormone (rhPTH) promotes bone mineral density and tendon-to-bone healing in humans and animals with rotator cuff tear. However, problems regarding repeated systemic rhPTH injections in humans exist. This study was conducted to evaluate the effect of topical rhPTH administration using three-dimensionally (3D) printed nanofiber sheets on tendon-to-bone healing in a rabbit RCT model

compared to that of direct topical rhPTH administration.

Materials and Methods: Eighty rabbits were randomly assigned to five groups (n = 16 each). To create the chronic RCT model, we induced complete supraspinatus tendon tears in both shoulders and left them untreated for 6 weeks. All transected tendons were repaired in a transosseous manner with saline injection in group A, hyaluronic acid (HA) injection in group B, 3D-printed nanofiber sheet fixation in group C, rhPTH and HA injection in group D, and 3D-printed rhPTH- and HA-soaked nanofiber sheet fixation in group E. Genetic (mRNA expression evaluation) and histological evaluations (hematoxylin and eosin and Masson's trichrome staining) were performed in half of the rabbits at 4 weeks post-repair. Genetic, histological, and biomechanical evaluations (mode of tear and load to failure) were performed in the remaining rabbits at 12 weeks.

Results: For genetic evaluation, group E showed a higher collagen type I alpha 1 expression level than did the other groups (P = .008) at 4 weeks. However, its expression level was downregulated, and there was no difference at 12 weeks. For histological evaluation, group E showed greater collagen fiber continuity, denser collagen fibers, and more mature tendon-to-bone junction than did the other groups (P = .001, P = .001, and P = .003, respectively) at 12 weeks. For biomechanical evaluation, group E showed a higher load-to-failure rate than did the other groups (P < .001) at 12 weeks.

Conclusion: Three-dimensionally printed rhPTH-soaked nanofiber sheet fixation can promote tendon-to-bone healing of chronic RCT.

Keyword: Recombinant human parathyroid hormone; Nanofiber sheet; 3D-printed; Tendon-to-bone healing; Chronic rotator cuff tear; Rabbit model

Student Number: 2020-37085

Contents

List of Figures

List of Tables

Chapter 1. Introduction

Rotator cuff tears (RCTs) are a common and progressive disease of the upper extremity that causes pain and disorders of the shoulder joint. Fortunately, given the rapid development of surgical techniques, satisfactory treatment outcomes have been acquired.[8,38] However, despite improvements in surgical techniques, postoperative healing failure remains a frequent complication, with the failure rates ranging from 11% to 94%.[21,31]

Numerous risk factors have been suspected to contribute to healing failure.[11] Additionally, osteoporosis is an independent prognostic factor for rotator cuff healing.[12] Recombinant human parathyroid hormone (rhPTH) was reported to have markedly enhanced the bone mineral density and healing of the rotator cuff.[15,24] As it is able to modulate calcium homeostasis by preventing calcium ion loss in vivo,[1,17,42] rhPTH has been a growing area of interest for biological agents to promote rotator cuff healing.[10,18,24,57]

Restoration of the tendon-to-bone enthesis to its original state after rotator cuff repair is crucial. The native rotator cuff insertion of the humeral head consists of four typical zones: tendon, unmineralized fibrocartilage, mineralized fibrocartilage, and bone. Precisely, rhPTH positively affects reconstruction of the fibrocartilage zone through the chondrogenic pathway.[29,43] Fibrocartilage formation and type I procollagen-producing cell production within the rotator cuff insertion could markedly increase after daily systemic rhPTH administration in

rats after rotator cuff repair.[24] Not only that, a clinical study reported that rhPTH could be a systemic treatment option that could markedly enhance tendon-to-bone healing after arthroscopic rotator cuff repair in patients with > 2-cm RCTs.[45]

However, systemic rhPTH treatment could induce several side effects.[36,40,50] Thus, topical rhPTH administration has stimulated considerable interest in many researchers evaluating the effect in animal models.[4,16,51] However, studies of topical rhPTH administration have mostly been limited to bone formation and bone mineral density,[4] and the effects on tendon-to-bone healing of the rotator cuff have been sparsely reported. The routes of topical administration have been reported, including direct injection using syringes, alginate scaffolds, and collagen sponges.[4,57] Nevertheless, research on the appropriate methods of topical rhPTH administration for rotator cuff healing remains insufficient, and the results are disputable. Nanofiber scaffolds are the latest finding in the field of biological material as a topical administration tool, because they can be used for specific drug-delivery applications and provide an environment of extracellular matrix (ECM) necessary for tendon healing.[47,54] Furthermore, nanofiber organization and alignment can be modulated during fabrication, which is suitable for the functional demands of the rotator cuff tendons.[34,37]

Therefore, we attempted to verify the effect of topical rhPTH administration using biomimetic nanofiber sheets for rotator cuff healing. We aimed to investigate the effect of three-dimensionally (3D) printed rhPTH-soaked nanofiber sheets on rotator cuff healing in a

rabbit chronic RCT model. We hypothesized that the use of 3D-printed rhPTH-soaked nanofiber sheets would support and improve rotator cuff healing compared to direct topical rhPTH administration.

Chapter 2. Materials and Methods

Animal care and all experimental procedures were performed in accordance with the guidelines approved by the Institutional Animal Care and Use Committee of the Clinical Research Institute of the senior author (J.H.O.) (IACUC No. BA-2006-297-048-01).

2.1. Three-Dimensionally Printed Nanofiber Sheet Fabrication

Preparation of the 3D printed nanofiber sheet was performed at the School of Mechanical Engineering, Pusan National University, Republic of Korea. A polycaprolactone (PCL; MW, 80000; Sigma-Aldrich, MO) solution dissolved in a 75/25 (volume ratio) mixture of dichloromethane (Samchun Pure Chemical, Republic of Korea) and dimethylformamide (Junsei Chemical, Japan) was used as the material for electrospinning. Electrospinning PCL solution was used at 14% concentration (weight-to-volume ratio). The electrospinning process was conducted as follows: PCL solution was infused with a disposable syringe and a metal needle (23-gauge) at a rate of 60 uL/min to form polymer drops. A voltage of 20 kV per 200 mm was applied to the tip of the needle to induce electrospinning.[49] The aligned nanofiber was harvested with an inclined-gap method, wherein the ejecting electrospun nanofiber was aligned in an electromagnetic field formed by two aluminum metal strips. The repulsive force between nanofibers

allowed the formation of a well-oriented nanofiber scaffold. The electrospinning time was set to 100 s. The electrospun nanofiber morphologies (Figure 1A) were confirmed using scanning electron microscopy. Subsequently, the PCL filament feedstock was printed using a homemade 3D printing system based on the mechanism of material extrusion. It was processed into a microstructured framework fused with a nanofiber sheet (Figure 1B). The framework stabilized the structure of the nanofiber sheet.

2.2. Carrier Selection

Hyaluronic acid (HA) was selected as the carrier for loading rhPTH. It is a highly viscous polysaccharide that plays a crucial role in organizing the ECM in the human body, which could be a desirable biomedical agent owing to its anti-inflammatory effects and stimulation of tendon-to-bone healing.[33] HA has also been investigated for use as a carrier of drugs, cells, and recently, proteins.[27,39] It should not denature the protein but release it in a prolonged period.[5] However, the nanofiber scaffold has been reported to have shown a rapid burst release at an early stage after implantation. Thus, HA played a highly important role as the rhPTH carrier herein to maintain the rhPTH concentration for a long period on the 3D-printed nanofiber sheet.[23]

2.3. Three-Dimensionally Printed rhPTH-Soaked Nanofiber Sheet Fabrication (Figure 2)

After 3D printing, a 1 mL 70% (volume/volume) ethanol solution (diluted from 96% [volume/volume] ethanol, with distilled water) was added to each sheet sample. Samples were treated for at least 30 min and were subsequently rinsed 5 times with 1 mL phosphate-buffered saline (PBS).[26] Subsequently, the 3D-printed nanofiber sheet was soaked thinly with a mixture of 20 μg rhPTH (Forteo; Eli Lilly, Indianapolis, IN) and 0.1 mL HA (Synovian; LG Life Sciences, Seoul, Republic of Korea).

2.4. Rabbit Allocation (Figure 3)

The sample size was determined via a power analysis as previously described.[30,53] With a minimum sample size, eight rabbits were required to detect a significant difference in the ultimate failure load (mean difference: 90 N; standard deviation: 40 N; α-error: 0.05; β-error: 0.2; dropout rate: 25%). We randomly allocated 80 female New Zealand White rabbits (average age, 6 months; weight, 3.5–4.0 kg) into five groups (16 rabbits per group): group A (repair + saline injection), group B (repair + HA injection), group C (repair + 3D-printed nanofiber sheet fixation), group D (repair + rhPTH and HA injection), and group E (repair + 3D-printed rhPTH- and HA-soaked nanofiber sheet fixation). All rabbits underwent bilateral surgical procedures, and a total of 160 shoulders were included herein. Each specimen harvested from half of the rabbits (8 rabbits per group) underwent

gene expression analysis and histological evaluation at 4 weeks post-repair. Each specimen harvested from the right shoulder of the remaining rabbits (8 rabbits per group) underwent gene expression analysis and histological evaluation at 12 weeks post-repair, while that harvested from the left shoulder underwent biomechanical evaluation at 12 weeks post-repair.

2.5. Surgical Procedure

All surgical procedures were performed by an experienced shoulder surgeon (J.H.). Under anesthesia and sterile conditions, a longitudinal incision was created between just proximal to the acromion process and greater tuberosity of the bilateral shoulder, and the deltoid muscle was retracted to expose the supraspinatus tendon. According to a previously reported process of creating chronic RCT models,[13] the supraspinatus tendon was transected using a sharp scalpel from the footprint on the greater tuberosity and wrapped with a silicone Penrose drain 10 mm in length (8 mm in outer diameter; Yushin Corp, Republic of Korea) to prevent adhesion to the surrounding soft tissue. Six weeks after supraspinatus tear induction, the Penrose drain around the torn supraspinatus tendon was removed, and the detached supraspinatus tendon was repaired using 2-0 Ticron (Tyco, Waltham, MA) using a transosseous technique at the footprint of the greater tuberosity. In detail, soft tissues surrounding the exposed greater tuberosity were ablated using a scalpel blade to create a bony bleeding bed. Two

transosseous tunnels were prepared at the articular margin of the supraspinatus footprint to the lateral humeral cortex. For reattachment of the torn tendon, the suture end was passed through the bone tunnels and tied to reconnect the supraspinatus tendon to its footprint. Subsequently, we injected 0.1 mL saline to the musculotendinous junction of bilateral supraspinatus in group A, 0.1 mL HA in group B, and mixture of 0.1 mL HA and 20 ug rhPTH in group D. In group C, we placed 3D-printed nanofiber sheet on the surface of tendon-to-bone repair site of bilateral shoulder. In group E, the 3D-printed rhPTH-soaked nanofiber sheet was placed in the same manner of group C (Figure 4). Herein, insufficient degradation of nanofiber taken into account, when placed into tendon-to-bone interface, we made the final decision to place 3D-printed nanofiber sheet on the surface of tendon-to-bone repair site.

The wound was closed in layers, co-opting the various layers. Postoperatively, the rabbits were housed individually and were not restricted to weight bearing or immobilized in any manner. To control pain, we injected meloxicam (Metacam, Boehringer Ingelheim Vetmedia), 0.3 mg/kg intramuscularly. Also, cefazolin was intramuscularly injected to prevent perioperative infection at a dose of 30 mg/kg post-surgery and every 24 h for 3 days.

2.6. Quantitative Real-Time Polymerase Chain Reaction (qRT-PCR)

Forty rabbits per timepoint (4 and 12 weeks post-repair) were anesthetized and humanely sacrificed with an intravenous injection of saturated potassium chloride solution (2 mmol/kg). A minimal specimen (3 x 3 mm2) of the repaired supraspinatus tendon was immediately frozen in liquid nitrogen and stored at −80°C after being harvested from each right shoulder for mRNA expression analysis.[32] RNeasy Mini Kit columns (Qiagen, Hilden, Germany) were used to extract RNA using the manufacturer's protocol. Total RNA from the tendon specimens was homogenized in tubes containing beads using TRIzol reagent (Invitrogen, Carlsbad, CA). One microgram of total RNA was reverse transcribed into complementary DNA using Maxime RT PreMix (iNtRON, Bio Inc., Sungnam, Republic of Korea). qRT-PCR was performed using the QuantStudio 6 Flex Real-Time PCR System (Applied Biosystems, Foster City, CA) with the SYBR Green PCR master mix (Applied Biosystems). The following protocol was used: denaturation at 95°C for 10 min, followed by 40 cycles of denaturation at 95°C for 15 s and annealing at 58°C for 1 min without extension. The denaturation and annealing steps were repeated to calculate the values of the linear phase. The relative gene expression levels were analyzed using the 2-ΔΔCT method with glyceraldehyde-3-phosphate dehydrogenase (GAPDH) as an internal reference.[35] Here, collagen type I alpha 1 (COL1A1) and collagen type III alpha 1 (COL3A1) mainly encode the major components of type I collagen and type III collagen, respectively. Bone morphogenetic protein 2 (BMP-2) plays an important role in bone and tendon development, and scleraxis (SCX) is

mainly expressed in the progenitors and cells of all tendon tissues. SRY-box 9 (SOX9) and aggrecan (ACAN) are essential transcription factors required for chondrocyte differentiation and cartilage formation (Table 1). The whole procedure were performed by an independent analyst who was blind to group allocation.

2.7. Histological Evaluation

At 4 and 12 weeks post-repair, the supraspinatus tendon specimens were processed as published previously for histological evaluation.[13,30,44] Tissues were embedded in paraffin after fixation in 10% neutral-buffered formalin overnight and sectioned into 5 mm-thick blocks for hematoxylin and eosin staining to assess tendon-to-bone healing at the repair site. Masson's trichrome staining was used to determine collagen fiber continuity, orientation, and density, which was performed on paraffin sections. And we also used the average of 10 measured values for quantitative analysis.

Each histological evaluation item, including collagen fiber continuity, orientation, density and tendon-to-bone interface maturation, was graded semi-quantitatively using a 4-stage system (grade 0 to 3) as previously reported.[13] The collagen fiber continuity stages and orientation were divided by percentage as follows: grade 0, 0%–24%; grade 1, 25%–49%; grade 2, 50%–74%; and grade 3, 75%–100%. Collagen fiber density was classified as very loose, loose, dense, and very dense (grades 0–3, respectively). Tendon-to-bone interface

maturation was graded from 0 to 3, which corresponded to poor, mild, moderate, or marked organization, respectively. For the statistical analysis, the response grades were given a numerical score of 1 for grade 0, 2 for grade 1, 3 for grade 2, and 4 for grade 3.

An Eclipse Ci-L microscope (Nikon, Tokyo, Japan) was used, and images were captured and acquired using a Nikon DS-U3 and NIS Elements BR 5.2 acquisition software (Nikon).

2.8. Biomechanical Evaluation

At 12 weeks post-repair, under adequate anesthesia and euthanasia, 40 specimens (eight specimens per group) comprising the humerus head with its attached supraspinatus tendon unit were harvested from the left shoulder for biomechanical evaluation using a universal material testing machine (AGS-X; Shimadzu, Kyoto, Japan). The machine consists of two subsections, including the fixation units of the humeral head and tendon. To form a right angle, we firmly fixed the supraspinatus tendon to this system along its anatomic direction to allow tensile loading (Figure 5). The parameters of the biomechanical evaluation were the mode of tear (insertional tear: mid-substance tear) and load-to-failure, which was measured as previously described.[44] Before the tensile test, the specimens were preloaded with a static preload at 5 N for 5 s, followed by five cycles of cyclic loading from 5 to 50 N at a loading rate of 15 N/s. Subsequently, they were elongated at a rate of 1 mm/s until failure. The load-to-failure rate of

displacement was determined as a value as previously described.[13] Data from the tensile load-to-failure testing were digitized and recorded using a personal computer-based data-acquisition system.

2.9. Statistical Analysis

For multiple-group comparisons, the Kruskal-Wallis test was used to evaluate the data from the PCR and biomechanical tests, followed by the post-hoc Mann – Whitney U test with Bonferroni correction. Histological categorical variables were analyzed by use of a Chi-square test for trend. All statistical analyses were performed by a specialized statistician in a blind manner using SPSS v.23.0 (SPSS, Inc., Chicago, IL), and P values of $< .05$ were considered statistically significant.

Chapter 3. Results

Data from eight rabbits were excluded from the final analysis. One rabbit in group A, two rabbits in group B, and two rabbits in group D showed active infection with purulent discharge at 4 weeks post-repair. At the same time, one rabbit in group C and two rabbits in group E died from an anesthetic accident. At the final evaluation, no rabbit had supraspinatus tendon dehiscence from the footprint in any of the groups.

3.1. qRT-PCR Analysis

Group E showed the highest COL1A1 mRNA expression level among all groups (P = .008) at 4 weeks post-repair. Furthermore, there were no differences in COL1A1 mRNA expression level among group A, B, C and D. However, the expression level showed no difference among the groups at 12 weeks post-repair (P = .074).

There were no significant differences in the mRNA expression levels of COL3A1, BMP-2, SCX, SOX9, and ACAN at either 4 or 12 weeks post-repair (all P > .05). The qRT-PCR analysis results are shown in Table 2.

3.2. Histological Evaluation

The results of the histological analysis according to the semi-

quantitative grading system are reported in Table 3. There were no apparent differences in any parameter among the groups at 4 weeks post-repair (P > .05).

However, collagen fiber continuity was greater in group E than in the other groups at 12 weeks post-repair (P = .001) (Figure 6A). Furthermore, group E showed denser collagen fibers and more mature tendon-to-bone junction than did the other groups (Density, maturation; P = .001 and .003, respectively) (Figure 6B). Meanwhile, there were no differences in variables mentioned above among group A, B, C and D. Although group E showed a higher orientation of collagen fibers, there was no significant difference compared to the other groups (P = .559).

3.3. Biomechanical Evaluation

At 12 weeks post-repair, the ultimate load-to-failure in each group was as follows (mean ± SD): group A, 108.2 ± 3.6 N; group B, 111.6 ± 6.8 N; group C, 118.8 ± 9.1 N; group D, 122.4 ± 10.0 N; and group E, 154.4 ± 18.0 N; group E showed the highest load-to-failure among all groups (P < .001) (Table 4 and Figure 7). Furthermore, there were no differences among group A, B, C and D.

The modes of tear in each group are listed in Table 4. Previously, the mode of mid-substance tear has been shown to be associated with better tendon-to-bone healing than the mode of insertional tear.52 There were six insertional tears and two midsubstance tears (25.0%) in

group A, five insertional tears and three midsubstance tears (37.5%) in group B, four insertional tears and four midsubstance tears (50.0%) in group C, five insertional tears and three midsubstance tears (37.5%) in group D, and two insertional tears and six midsubstance tears (75.0%) in group E (P = .339).

Chapter 4. Discussion

Herein, we found that topical administration of 3D-printed rhPTH-soaked nanofiber sheets on the torn supraspinatus tendon improved the COL1A1 expression level at an early stage post-repair and significantly enhanced the histological and biomechanical outcomes at 12 weeks in the rabbit chronic RCT model compared to direct topical rhPTH application. Taken together, these findings support our hypothesis that 3D-printed rhPTH-soaked nanofiber sheet usage would improve tendon-to-bone healing of chronic RCTs.

In fact, successful tendon-to-bone healing requires solid tendon fixation on the previous footprint during repair and effective tendon-to-bone junction restoration through the new bone formation and remodeling.[3,20] Thus, desirable tendon-to-bone healing outcomes could be achieved with the effect of rhPTH (binding to the rhPTH receptor in mesenchymal stem cells, osteocytes, and osteoblasts[6]) on serum calcium regulation to maintain good bone mineral density. Daily subcutaneous rhPTH injections could improve the density of the bone and blood vessels and collagen fiber orientation from the day of repair in rats.[24] Similarly, systemic rhPTH treatment could markedly enhance tendon-to-bone healing after arthroscopic rotator cuff repair in humans, especially with RCTs larger than 2 cm.[45]

Unfortunately, systemic rhPTH administration remains inconvenient and causes side effects in humans; therefore, topical rhPTH administration during surgical repair has gained attention. Furthermore,

research on topical rhPTH administration via different carriers greatly focused on tendon and bone healing.[2,4,56,57] Owing to our encouraging study results, we could verify that tendon-to-bone healing would be enhanced by the use of topical 3D-printed rhPTH-soaked nanofiber sheets during rotator cuff tendon repair, although we did not compare it with the traditional systemic rhPTH injection.

We fabricated the nanofiber sheet using electrospinning technique. The electrospinning extrudes and erupts the polymer solution jets under a strong electric field, thereby producing the long continuous fibers with sub-micrometer scale diameter in a very productive way.[19,49] In the scaffold-based tissue engineering, electrospun nanofibers play an important role in novel delivery application of cells, nucleic acids, and proteins.[48] In terms of topically effective protein delivery including hormones, growth factors, and enzymes in vivo, designing a controlled delivery system that could obtain desired concentrations of the key material and maintain its biological activity is necessary. Both in vivo and in vitro experiments have demonstrated that nanofiber scaffolds could be used as a long-term delivery system for various factors and express biological signals to modulate tissue regeneration with respect to their ultrathin fiber diameter and large surface-volume ratio.[28] Nanofiber scaffolds have been reported to effectively augment tendon-to-bone integration and improve the gradient microstructure in a rabbit extra-articular model by inducing new bone formation, increasing the area of fibrocartilage, and improving collagen organization and maturation.[7] Furthermore,

nanofiber scaffolds loaded with growth factor β 3 have shown advantages in biomechanical stability of the repair site in a rat chronic RCT model.[46] Therefore, we believe that the 3D-printed nanofiber sheet developed herein could be applied as a delivery application method of rhPTH without causing complications.

Local rhPTH application using absorbable scaffolds could enhance the histological, immunohistochemical, and biomechanical outcomes of tendon-to-bone healing, which is also similar to the effect of systemic rhPTH injection in rat RCT models.[57] Although our rhPTH administration method was different, we found that topical rhPTH administration using a nanofiber-based sheet could significantly improve the continuity and density of collagen fibers and maturation at the tendon-to-bone junction. The underlying mechanism by which topical rhPTH administration enhances the tendon-to-bone healing process has not yet been revealed. However, our study provides an initial understanding that controlled rhPTH release from the nanofiber-based sheet could stimulate normal transition site formation, which achieves better rotator cuff tendon healing. In other words, topical rhPTH administration might possess the advantage of controlled release and rhPTH concentration maintenance in the tendon-to-bone junction compared to direct topical rhPTH injections to the repaired tendon, which temporally increases the rhPTH levels. Furthermore, the rhPTH ligand-receptor binding efficiency may increase when rhPTH acts as a local or paracrine factor in the treatment site.[9]

Herein, we evaluated the mRNA expression levels of various genes.

At 4 weeks post-repair, the COL1A1 expression level in group E was significantly higher than that in the other groups. Generally, rhPTH can regulate the gene expression of types 1 and 3 collagen, which play a key role in the deposition of ECM components, and type 1 collagen was noted earlier than type 3 collagen at the early stage post-injury.[22,55] This coincides with our genetic evaluation results. As the primary component of the ECM of both the tendon and its insertion, type 1 collagen is important for rotator cuff properties, and its regeneration could lead to better tendon-to-bone healing at a later stage. Furthermore, we thought it could cause more collagen fiber formation and histological integrity to achieve better biomechanical results in group E at 12 weeks post-repair than in the other groups. HA and nanofiber scaffolds themselves were reported as biological augmentations to support rotator cuff healing in previous studies.[25,41] Honda et al. demonstrated the superior effect of HA on rotator cuff healing through injecting it into the bone groove on the greater tuberosity in the repaired site, while comparing with injecting PBS. However, it was probably the injection manner of HA which had resulted in different outcome that there were no significant differences in any analysis in group B (HA was injected into musculotendinous portion as carrier of rhPTH), compared to other control groups. Furthermore, nanofiber scaffold, made up of PCL or poly(L-lactide-co-glycolide) (PLGA), was also reported that it could play a biological material role in providing an environment of ECM necessary for tendon-to-bone healing, when applied between tendon and bone

interface. However, to observe the effect of topical administrated rhPTH on rotator cuff healing, nanofiber sheet, treated as topical scaffold of rhPTH, was not only placed on the surface of tendon-to-bone repair site for group C and E in this study, but group C did not show significant differences in any analysis, compared to other control groups. On the other hand, the mixture of rhPTH and HA were injected for group D, and there were no significant differences in any analysis, compared to other control groups. Generally, these results suggest that topical rhPTH administration using 3D-printed nanofiber sheets could enhance tendon-to-bone healing after rotator cuff repair in rabbits and has better effects than direct topical rhPTH administration with injection manner.

To our knowledge, this is the first study to evaluate the effect of topical rhPTH administration with 3D-printed nanofiber sheet fixation on tendon-to-bone healing in rabbit chronic RCT models. However, this study had several limitations. First, owing to the animal experimental study design, this study was unable to demonstrate that topical rhPTH administration is also effective in humans with RCTs. There are various differences between rabbits and humans in terms of healing potential and anatomic force mechanism to the glenohumeral joint, regardless of weight bearing; thus, future investigations on this topic are necessary. Second, the rabbit chronic RCT model used was created artificially, reattaching the supraspinatus tendon from the footprint 6 weeks after detaching, contrary to human cases, which are mainly a long-term degenerative disease. However, we have already

conducted several animal experiments on chronic rotator cuff tendon repair in rabbit models;[13,14,30,32,44] therefore, we think that this is the suitable model of chronic RCTs in humans. Third, we did not evaluate the effect of rhPTH with 3D-printed nanofiber sheet fixation without HA or HA with 3D-printed nanofiber sheet fixation without rhPTH on rotator cuff healing as a stand-alone control group. To avoid rapid burst release of rhPTH from the sheet, we applied HA as a carrier to ensure sustained release. Fourth, the in vitro degradation of 3D-printed PCL nanofiber sheets has not been investigated in detail. Although PCL degradation requires more than 1 year, and total degradation requires approximately 3 or 4 years, the sheets applied herein were thin, with minimal tension affecting the biomechanical results. Meanwhile, group C (only nanofiber sheet group) did not appear the significant difference in biomechanical test, compared to group A (saline group), so we could identify again that the nanofiber sheet did not play an interfering factor in biomechanical test. Fifth, we did not check the condition of rhPTH sustained release from the 3D-printed nanofiber sheet in vitro, the rhPTH concentration volume in vivo over time and the effect of other rhPTH concentrations. However, various related studies demonstrated previously that nanofibrous scaffold itself without any carrier could sustainably release and deliver the specific drug, growth factor and protein.[47,54] Furthermore, applying the HA as carrier in this study, we could firmly believe the sustained release function of 3D-printed nanofiber sheet. Anyway, to compensate the limitation, further studies of this issue are ongoing in

our laboratory. Sixth, as this study was based on the assumption that there was any rhPTH absorption by peripheral tissues to enter systemic circulation through the topical administration, the extra data on the rhPTH levels in vivo were not evaluated when the experimental rabbits were euthanized. Finally, it could be much better to observe the tendon-to-bone healing, if we performed microCT analysis to quantify the improvement of bone quality at supraspinatus tendon footprint.

Chapter 5. Conclusion

Three-dimensionally printed rhPTH-soaked nanofiber sheet fixation can promote tendon-to-bone healing in rabbits with chronic RCTs. If the safety and compatibility of 3D-printed rhPTH-soaked nanofiber sheets are found to be reliable for humans, their use would be further investigated in clinical trials.

References

1. Andreassen TT, Ejersted C, Oxlund H. Intermittent parathyroid hormone (1-34) treatment increases callus formation and mechanical strength of healing rat fractures. J Bone Miner Res 1999;14(6):960-8. doi:10.1359/jbmr.1999.14.6.960 PMID:10352105
2. Arrighi I, Mark S, Alvisi M, von Rechenberg B, Hubbell JA, Schense JC. Bone healing induced by local delivery of an engineered parathyroid hormone prodrug. Biomaterials 2009;30(9):1763-71. doi:10.1016/j.biomaterials.2008.12.023 PMID:19124152
3. Atesok K, Fu FH, Wolf MR, Ochi M, Jazrawi LM, Doral MN, et al. Augmentation of tendon-to-bone healing. J Bone Joint Surg Am 2014;96(6):513-21. doi:10.2106/JBJS.M.00009 PMID:24647509
4. Auersvald CM, Santos FR, Nakano MM, Leoni GB, de Sousa Neto MD, Scariot R, et al. The local administration of parathyroid hormone encourages the healing of bone defects in the rat calvaria: Micro-computed tomography, histological and histomorphometric evaluation. Arch Oral Biol 2017;79:14-9. doi:10.1016/j.archoralbio.2017.02.016 PMID:28282513
5. Bayer IS. Hyaluronic Acid and Controlled Release: A Review. Molecules 2020;25(11). doi:10.3390/molecules25112649 PMID:32517278
6. Bi F, Shi Z, Jiang S, Guo P, Yan S. Intermittently administered

parathyroid hormone [1-34] promotes tendon-bone healing in a rat model. Int J Mol Sci 2014;15(10):17366-79. doi:10.3390/ijms151017366 PMID:25268612

7. Cai J, Wang J, Ye K, Li D, Ai C, Sheng D, et al. Dual-layer aligned-random nanofibrous scaffolds for improving gradient microstructure of tendon-to-bone healing in a rabbit extra-articular model. Int J Nanomedicine 2018;13:3481-92. doi:10.2147/IJN.S165633 PMID:29950830

8. Carbonel I, Martinez AA, Aldea E, Ripalda J, Herrera A. Outcome and structural integrity of rotator cuff after arthroscopic treatment of large and massive tears with double row technique: a 2-year followup. Adv Orthop 2013;2013:914148. doi:10.1155/2013/914148 PMID:23533788

9. Chen H, Frankenburg EP, Goldstein SA, McCauley LK. Combination of local and systemic parathyroid hormone enhances bone regeneration. Clin Orthop Relat Res 2003(416):291-302. doi:10.1097/01.blo.0000079443.64912.18 PMID:14646773

10. Chen X, Giambini H, Ben-Abraham E, An KN, Nassr A, Zhao C. Effect of Bone Mineral Density on Rotator Cuff Tear: An Osteoporotic Rabbit Model. PLoS One 2015;10(10):e0139384. doi:10.1371/journal.pone.0139384 PMID:26466092

11. Cho NS, Rhee YG. The factors affecting the clinical outcome and integrity of arthroscopically repaired rotator cuff tears of the shoulder. Clin Orthop Surg 2009;1(2):96-104.

doi:10.4055/cios.2009.1.2.96 PMID:19885061

12. Chung SW, Oh JH, Gong HS, Kim JY, Kim SH. Factors affecting rotator cuff healing after arthroscopic repair: osteoporosis as one of the independent risk factors. Am J Sports Med 2011;39(10):2099-107. doi:10.1177/0363546511415659 PMID:21813440

13. Chung SW, Park H, Kwon J, Choe GY, Kim SH, Oh JH. Effect of Hypercholesterolemia on Fatty Infiltration and Quality of Tendon-to-Bone Healing in a Rabbit Model of a Chronic Rotator Cuff Tear: Electrophysiological, Biomechanical, and Histological Analyses. Am J Sports Med 2016;44(5):1153-64. doi:10.1177/0363546515627816 PMID:26912283

14. Chung SW, Song BW, Kim YH, Park KU, Oh JH. Effect of platelet-rich plasma and porcine dermal collagen graft augmentation for rotator cuff healing in a rabbit model. Am J Sports Med 2013;41(12):2909-18. doi:10.1177/0363546513503810 PMID:24047553

15. Compston JE. Skeletal actions of intermittent parathyroid hormone: effects on bone remodelling and structure. Bone 2007;40(6):1447-52. doi:10.1016/j.bone.2006.09.008 PMID:17045858

16. Dang M, Koh AJ, Jin X, McCauley LK, Ma PX. Local pulsatile PTH delivery regenerates bone defects via enhanced bone remodeling in a cell-free scaffold. Biomaterials 2017;114:1-9. doi:10.1016/j.biomaterials.2016.10.049 PMID:27835763

17. Dempster DW, Cosman F, Parisien M, Shen V, Lindsay R. Anabolic actions of parathyroid hormone on bone. Endocr Rev 1993;14(6):690-709. doi:10.1210/edrv-14-6-690 PMID:8119233

18. Duchman KR, Goetz JE, Uribe BU, Amendola AM, Barber JA, Malandra AE, et al. Delayed administration of recombinant human parathyroid hormone improves early biomechanical strength in a rat rotator cuff repair model. J Shoulder Elbow Surg 2016;25(8):1280-7. doi:10.1016/j.jse.2015.12.016 PMID:26948004

19. Reneker DH, Chun I. Nanometre diameter fibres of polymer, produced by electrospinning. Nanotechnology 1996;7:216–23. doi:10.1088/0957-4484/7/3/009

20. Galanopoulos I, Ilias A, Karliaftis K, Papadopoulos D, Ashwood N. The Impact of Re-tear on the Clinical Outcome after Rotator Cuff Repair Using Open or Arthroscopic Techniques - A Systematic Review. Open Orthop J 2017;11:95-107. doi:10.2174/1874325001711010095 PMID:28400878

21. Galatz LM, Ball CM, Teefey SA, Middleton WD, Yamaguchi K. The outcome and repair integrity of completely arthroscopically repaired large and massive rotator cuff tears. J Bone Joint Surg Am 2004;86(2):219-24. doi:10.2106/00004623-200402000-00002 PMID:14960664

22. Galloway MT, Lalley AL, Shearn JT. The role of mechanical loading in tendon development, maintenance, injury, and repair.

J Bone Joint Surg Am 2013;95(17):1620-8. doi:10.2106/JBJS.L.01004 PMID:24005204

23. Gentile P, Nandagiri VK, Pabari R, Daly J, Tonda-Turo C, Ciardelli G, et al. Influence of Parathyroid Hormone-Loaded PLGA Nanoparticles in Porous Scaffolds for Bone Regeneration. Int J Mol Sci 2015;16(9):20492-510. doi:10.3390/ijms160920492 PMID:26343649

24. Hettrich CM, Beamer BS, Bedi A, Deland K, Deng XH, Ying L, et al. The effect of rhPTH on the healing of tendon to bone in a rat model. J Orthop Res 2012;30(5):769-74. doi:10.1002/jor.22006 PMID:22068696

25. Honda H, Gotoh M, Kanazawa T, Ohzono H, Nakamura H, Ohta K, et al. Hyaluronic Acid Accelerates Tendon-to-Bone Healing After Rotator Cuff Repair. Am J Sports Med 2017;45(14):3322-30. doi:10.1177/0363546517720199 PMID:28872895

26. Horakova J, Klicova M, Erben J, Klapstova A, Novotny V, Behalek L, et al. Impact of Various Sterilization and Disinfection Techniques on Electrospun Poly-epsilon-caprolactone. ACS Omega 2020;5(15):8885-92. doi:10.1021/acsomega.0c00503 PMID:32337451

27. Huang G, Huang H. Application of hyaluronic acid as carriers in drug delivery. Drug Deliv 2018;25(1):766-72. doi:10.1080/10717544.2018.1450910 PMID:29536778

28. Ji W, Sun Y, Yang F, van den Beucken JJ, Fan M, Chen Z, et al. Bioactive electrospun scaffolds delivering growth factors and

genes for tissue engineering applications. Pharm Res 2011;28(6):1259-72. doi:10.1007/s11095-010-0320-6 PMID:21088985

29. Kakar S, Einhorn TA, Vora S, Miara LJ, Hon G, Wigner NA, et al. Enhanced chondrogenesis and Wnt signaling in PTH-treated fractures. J Bone Miner Res 2007;22(12):1903-12. doi:10.1359/jbmr.070724 PMID:17680724

30. Kwon J, Kim YH, Rhee SM, Kim TI, Lee J, Jeon S, et al. Effects of Allogenic Dermal Fibroblasts on Rotator Cuff Healing in a Rabbit Model of Chronic Tear. Am J Sports Med 2018;46(8):1901-8. doi:10.1177/0363546518770428 PMID:29746144

31. Le BT, Wu XL, Lam PH, Murrell GA. Factors predicting rotator cuff retears: an analysis of 1000 consecutive rotator cuff repairs. Am J Sports Med 2014;42(5):1134-42. doi:10.1177/0363546514525336 PMID:24748610

32. Lee JH, Kim YH, Rhee SM, Han J, Jeong HJ, Park JH, et al. Rotator Cuff Tendon Healing Using Human Dermal Fibroblasts: Histological and Biomechanical Analyses in a Rabbit Model of Chronic Rotator Cuff Tears. Am J Sports Med 2021;49(13):3669-79. doi:10.1177/03635465211041102 PMID:34554882

33. Li H, Ge Y, Zhang P, Wu L, Chen S. The effect of layer-by-layer chitosan-hyaluronic acid coating on graft-to-bone healing of a poly(ethylene terephthalate) artificial ligament. J Biomater

Sci Polym Ed 2012;23(1-4):425-38.
doi:10.1163/092050610X551989 PMID:21255485

34. Li WJ, Mauck RL, Cooper JA, Yuan X, Tuan RS. Engineering controllable anisotropy in electrospun biodegradable nanofibrous scaffolds for musculoskeletal tissue engineering. J Biomech 2007;40(8):1686-93.
doi:10.1016/j.jbiomech.2006.09.004 PMID:17056048

35. Livak KJ, Schmittgen TD. Analysis of relative gene expression data using real-time quantitative PCR and the 2(-Delta Delta C(T)) Method. Methods 2001;25(4):402-8.
doi:10.1006/meth.2001.1262 PMID:11846609

36. Luigetti M, Capone F, Monforte M, Di Lazzaro V. Muscle cramps and weakness after teriparatide therapy: a new drug-induced myopathy? Muscle Nerve 2013;47(4):615.
doi:10.1002/mus.23661 PMID:23322619

37. Ma Z, Kotaki M, Inai R, Ramakrishna S. Potential of nanofiber matrix as tissue-engineering scaffolds. Tissue Eng 2005;11(1-2):101-9. doi:10.1089/ten.2005.11.101 PMID:15738665

38. Melillo AS, Savoie FH, 3rd, Field LD. Massive rotator cuff tears: debridement versus repair. Orthop Clin North Am 1997;28(1):117-24. doi:10.1016/s0030-5898(05)70269-8 PMID: 9024436

39. Mero A, Campisi M, Caputo M, Cuppari C, Rosato A, Schiavon O, et al. Hyaluronic Acid as a Protein Polymeric Carrier: An Overview and a Report on Human Growth Hormone. Curr Drug

Targets 2015;16(13):1503-11.
doi:10.2174/1389450116666150107151906 PMID:25563593

40. Migliaccio S, Resmini G, Buffa A, Fornari R, Di Pietro G, Cerocchi I, et al. Evaluation of persistence and adherence to teriparatide treatment in patients affected by severe osteoporosis (PATT): a multicenter observational real life study. Clin Cases Miner Bone Metab 2013;10(1):56-60. doi:10.11138/ccmbm/2013.10.1.056 PMID:23858313

41. Moffat KL, Kwei AS, Spalazzi JP, Doty SB, Levine WN, Lu HH. Novel nanofiber-based scaffold for rotator cuff repair and augmentation. Tissue Eng Part A 2009;15(1):115-26. doi:10.1089/ten.tea.2008.0014 PMID:18788982

42. Murray TM, Rao LG, Divieti P, Bringhurst FR. Parathyroid hormone secretion and action: evidence for discrete receptors for the carboxyl-terminal region and related biological actions of carboxyl- terminal ligands. Endocr Rev 2005;26(1):78-113. doi:10.1210/er.2003-0024 PMID:15689574

43. Nakazawa T, Nakajima A, Shiomi K, Moriya H, Einhorn TA, Yamazaki M. Effects of low-dose, intermittent treatment with recombinant human parathyroid hormone (1-34) on chondrogenesis in a model of experimental fracture healing. Bone 2005;37(5):711-9. doi:10.1016/j.bone.2005.06.013 PMID:16143574

44. Oh JH, Chung SW, Kim SH, Chung JY, Kim JY. 2013 Neer Award: Effect of the adipose-derived stem cell for the improvement of

fatty degeneration and rotator cuff healing in rabbit model. J Shoulder Elbow Surg 2014;23(4):445-55. doi:10.1016/j.jse.2013.07.054 PMID:24129058

45. Oh JH, Kim DH, Jeong HJ, Park JH, Rhee SM. Effect of Recombinant Human Parathyroid Hormone on Rotator Cuff Healing After Arthroscopic Repair. Arthroscopy 2019;35(4):1064-71. doi:10.1016/j.arthro.2018.11.038 PMID:30857903

46. Reifenrath J, Wellmann M, Kempfert M, Angrisani N, Welke B, Gniesmer S, et al. TGF-beta3 Loaded Electrospun Polycaprolacton Fibre Scaffolds for Rotator Cuff Tear Repair: An in Vivo Study in Rats. Int J Mol Sci 2020;21(3). doi:10.3390/ijms21031046 PMID:32033294

47. Riggin CN, Qu F, Kim DH, Huegel J, Steinberg DR, Kuntz AF, et al. Electrospun PLGA Nanofiber Scaffolds Release Ibuprofen Faster and Degrade Slower After In Vivo Implantation. Ann Biomed Eng 2017;45(10):2348-59. doi:10.1007/s10439-017-1876-7 PMID:28653294

48. Stojanov S, Berlec A. Electrospun Nanofibers as Carriers of Microorganisms, Stem Cells, Proteins, and Nucleic Acids in Therapeutic and Other Applications. Front Bioeng Biotechnol 2020;8:130. doi:10.3389/fbioe.2020.00130 PMID:32158751

49. Teo WE, Ramakrishna S. A review on electrospinning design and nanofibre assemblies. Nanotechnology 2006;17(14):R89-R106. doi:10.1088/0957-4484/17/14/R01 PMID:19661572

50. Thiruchelvam N, Randhawa J, Sadiek H, Kistangari G. Teriparatide induced delayed persistent hypercalcemia. Case Rep Endocrinol 2014;2014:802473. doi:10.1155/2014/802473 PMID:25202461

51. Tokunaga K, Seto H, Ohba H, Mihara C, Hama H, Horibe M, et al. Topical and intermittent application of parathyroid hormone recovers alveolar bone loss in rat experimental periodontitis. J Periodontal Res 2011;46(6):655-62. doi:10.1111/j.1600-0765.2011.01386.x PMID:21722135

52. Trudel G, Ramachandran N, Ryan SE, Rakhra K, Uhthoff HK. Supraspinatus tendon repair into a bony trough in the rabbit: mechanical restoration and correlative imaging. J Orthop Res 2010;28(6):710-5. doi:10.1002/jor.21045 PMID:19953603

53. Uhthoff HK, Seki M, Backman DS, Trudel G, Himori K, Sano H. Tensile strength of the supraspinatus after reimplantation into a bony trough: an experimental study in rabbits. J Shoulder Elbow Surg 2002;11(5):504-9. doi:10.1067/mse.2002.126760 PMID:12378172

54. Wang X, Ding B, Li B. Biomimetic electrospun nanofibrous structures for tissue engineering. Mater Today (Kidlington) 2013;16(6):229-41. doi:10.1016/j.mattod.2013.06.005 PMID:25125992

55. Williams IF, McCullagh KG, Silver IA. The distribution of types I and III collagen and fibronectin in the healing equine tendon. Connect Tissue Res 1984;12(3-4):211-27.

doi:10.3109/03008208409013684 PMID:6478822

56. Wojda SJ, Marozas IA, Anseth KS, Yaszemski MJ, Donahue SW. Thiol-ene Hydrogels for Local Delivery of PTH for Bone Regeneration in Critical Size defects. J Orthop Res 2020;38(3):536-44. doi:10.1002/jor.24502 PMID:31709588

57. Yoon JP, Chung SW, Jung JW, Lee YS, Kim KI, Park GY, et al. Is a Local Administration of Parathyroid Hormone Effective to Tendon-to-Bone Healing in a Rat Rotator Cuff Repair Model? J Orthop Res 2020;38(1):82-91. doi:10.1002/jor.24452 PMID:31441073

Figure legend and Figures

Figure 1. (A) Scanning electron microscopy images of polycaprolactone nanofibers and (B) the final morphology and size of the three-dimensionally printed nanofiber sheet.

A

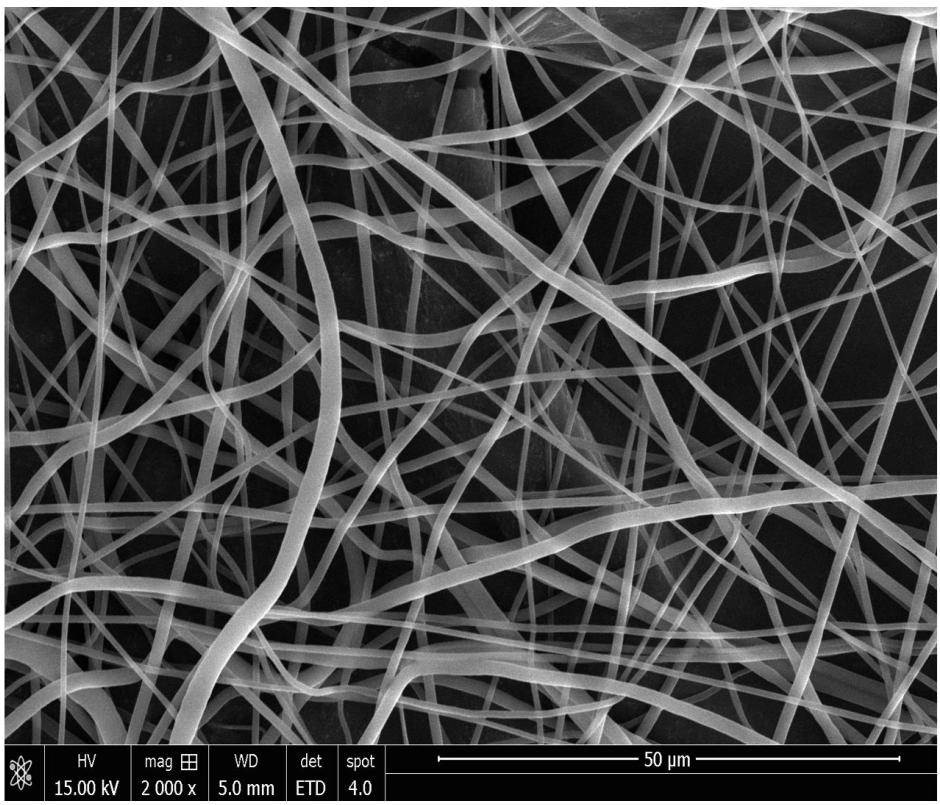

B

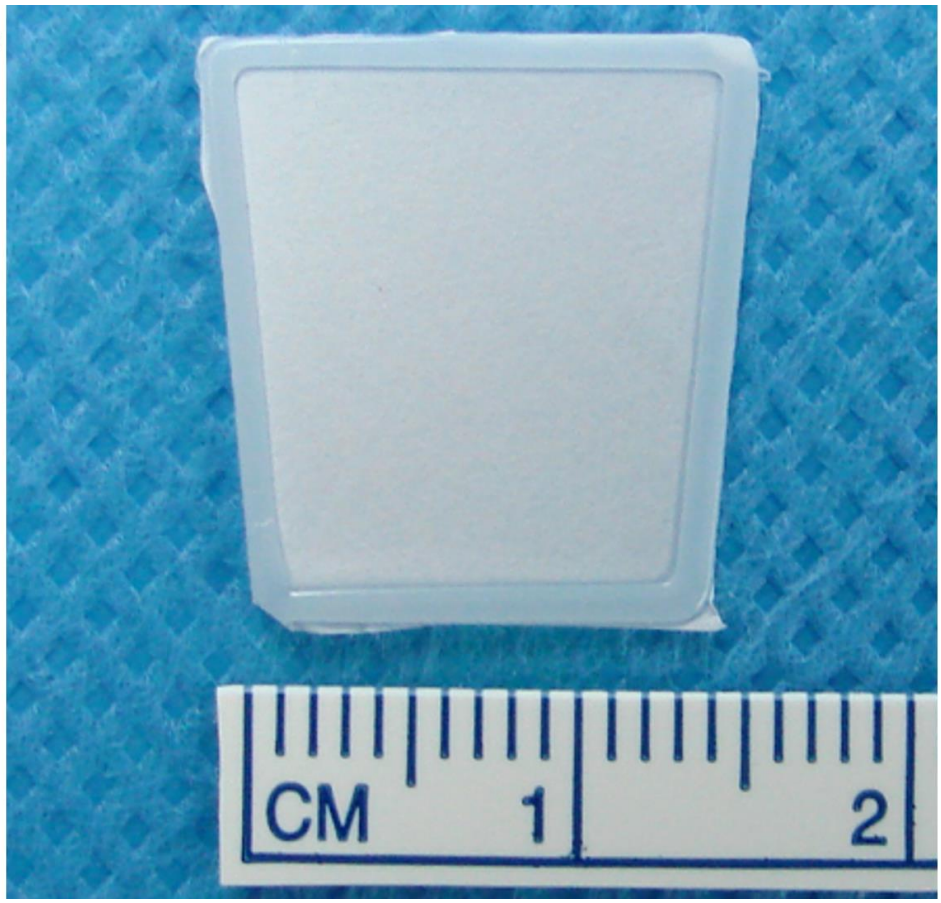

Figure 2. Final morphology of the three-dimensionally printed parathyroid hormone-soaked nanofiber sheet.

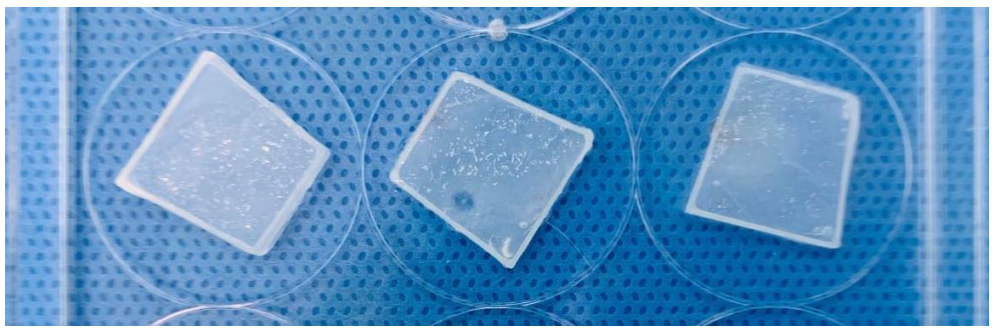

Figure 3. Flowchart of the study design. HA, hyaluronic acid; rhPTH, recombinant human parathyroid hormone

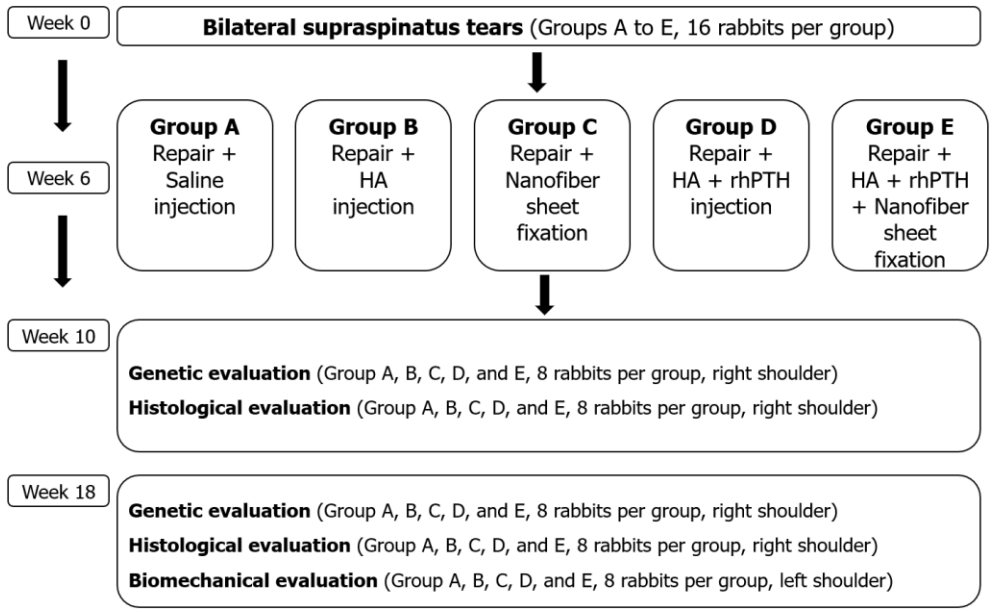

Figure 4. Fixation image of the three-dimensionally printed parathyroid hormone-soaked nanofiber sheet on the tendon-to-bone connection site when the torn supraspinatus tendon was repaired.

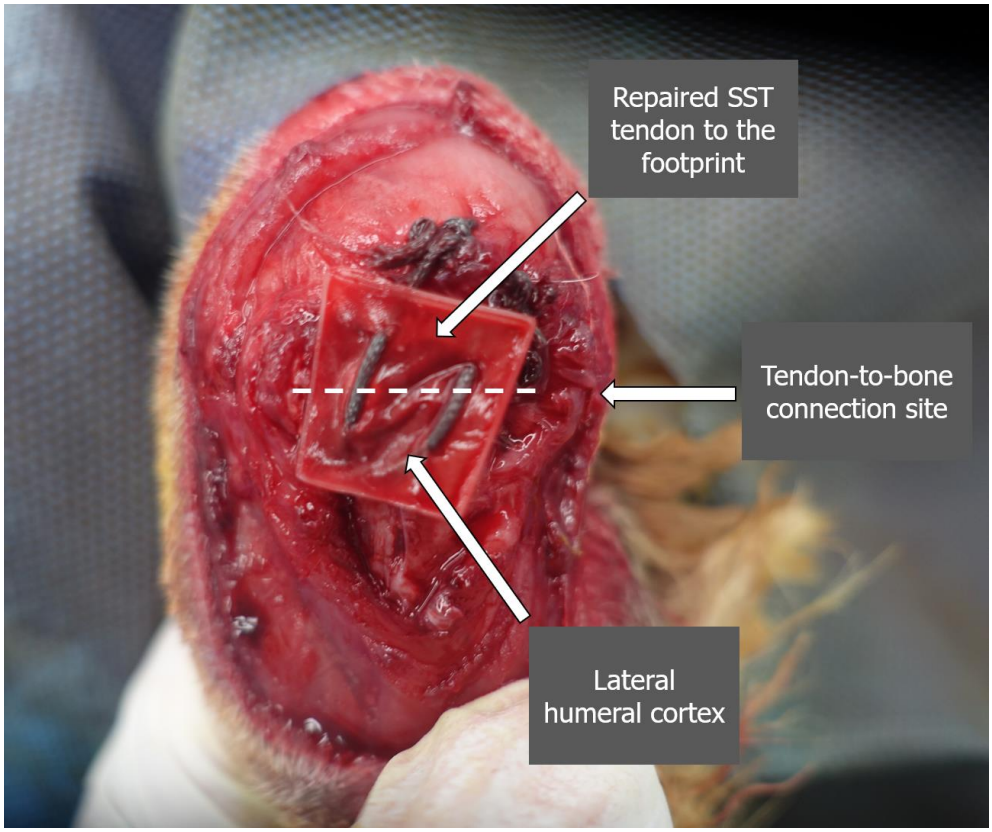

Figure 5. (A) The parameters of the biomechanical evaluation were tested using a custom fixture clamping system and a universal material testing machine. (B) The humeral head was firmly fixed to the humeral head fixation unit, and the supraspinatus tendon was emerged through the hole. The supraspinatus tendon was fixed to the upper clamping unit along its anatomic direction to allow tensile loading and tendon-to-bone interface, forming a right angle.

A

B

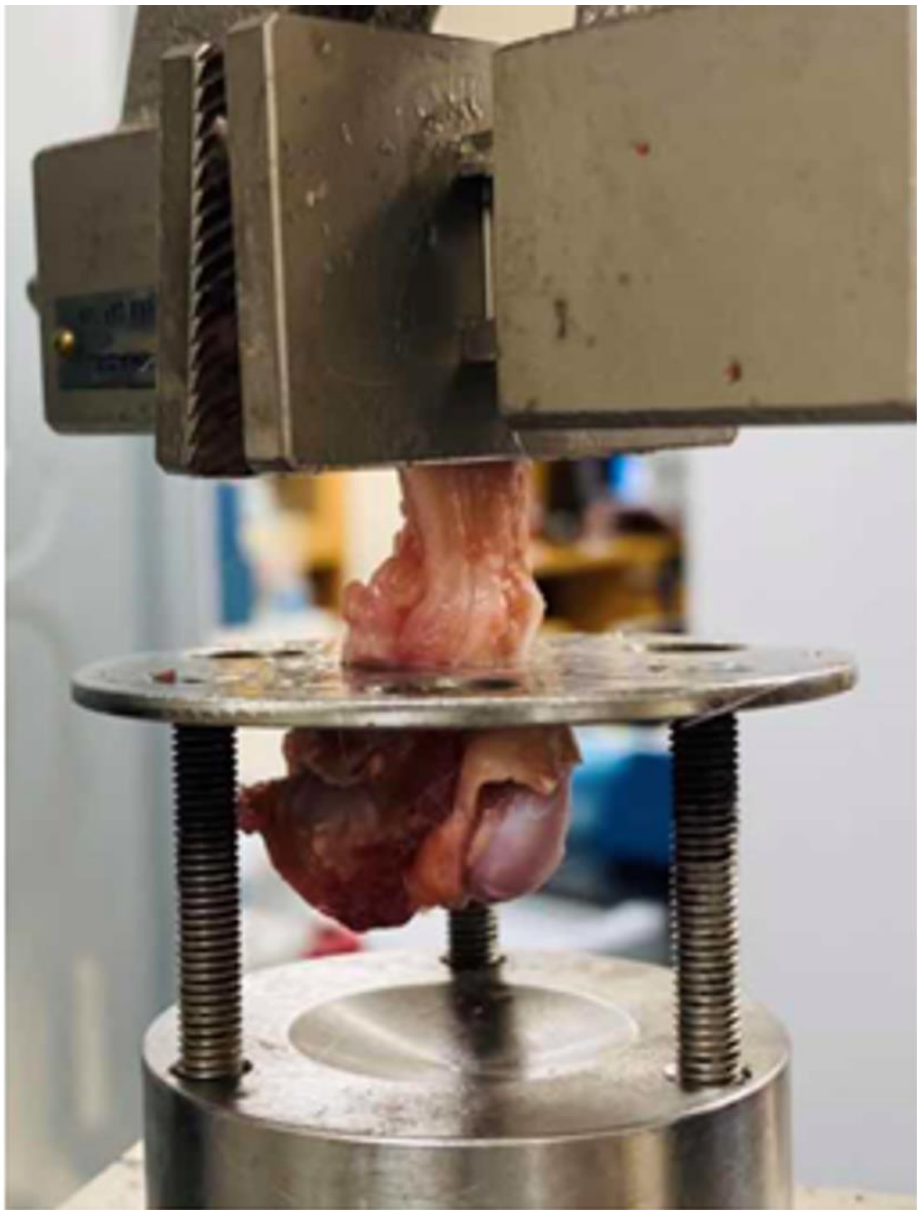

Figure 6. (A) Representative photomicrographs showing the tendon-to-bone junction stained with hematoxylin and eosin (magnification × 40) at 4 and 12 weeks after repair. At 12 weeks after repair, group E showed better collagen fiber continuity than did the other groups ($P < .001$). (B) Representative photomicrographs showing the tendon-to-bone junction stained with Masson's trichrome (magnification × 40) at 4 and 12 weeks after repair. At 12 weeks after repair, group E showed more dense depositions and organized alignment of collagen fibers and better maturation of the tendon-to-bone junction than did the other groups ($P < .001$).

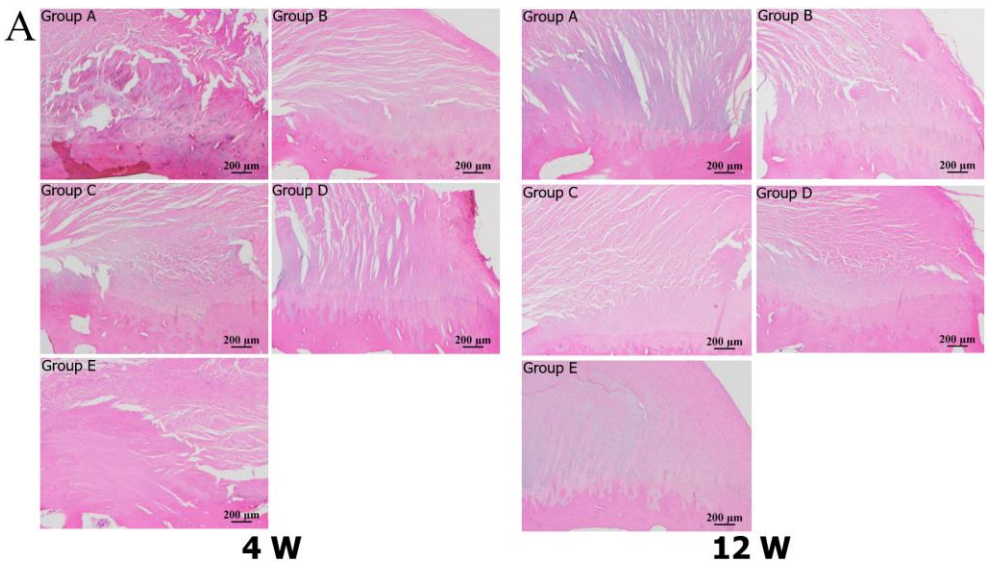

B

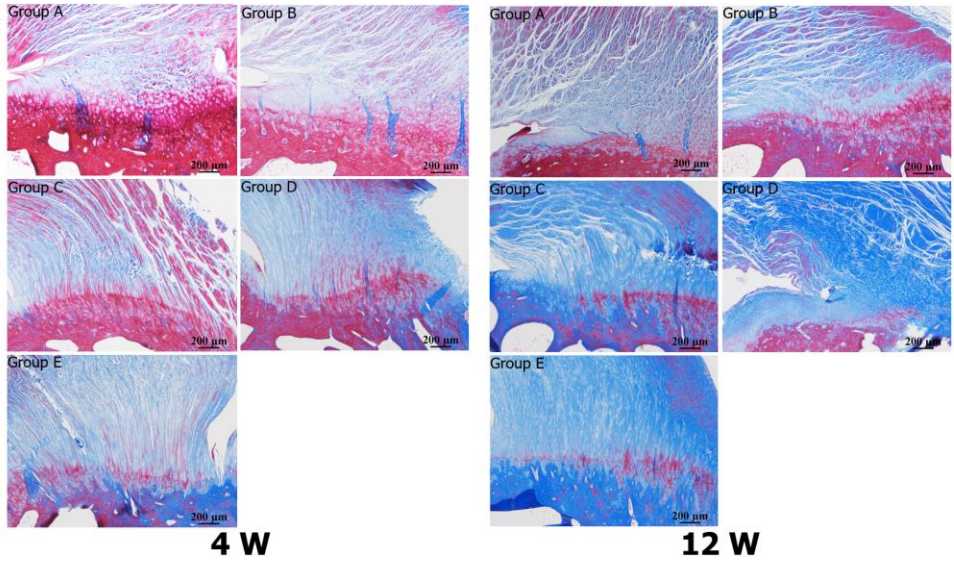

Figure 7. Load-to-failure of the repaired tissues in the biomechanical evaluation. Group E showed a significantly higher load-to-failure than did the other groups (P < .001).

*Significantly different

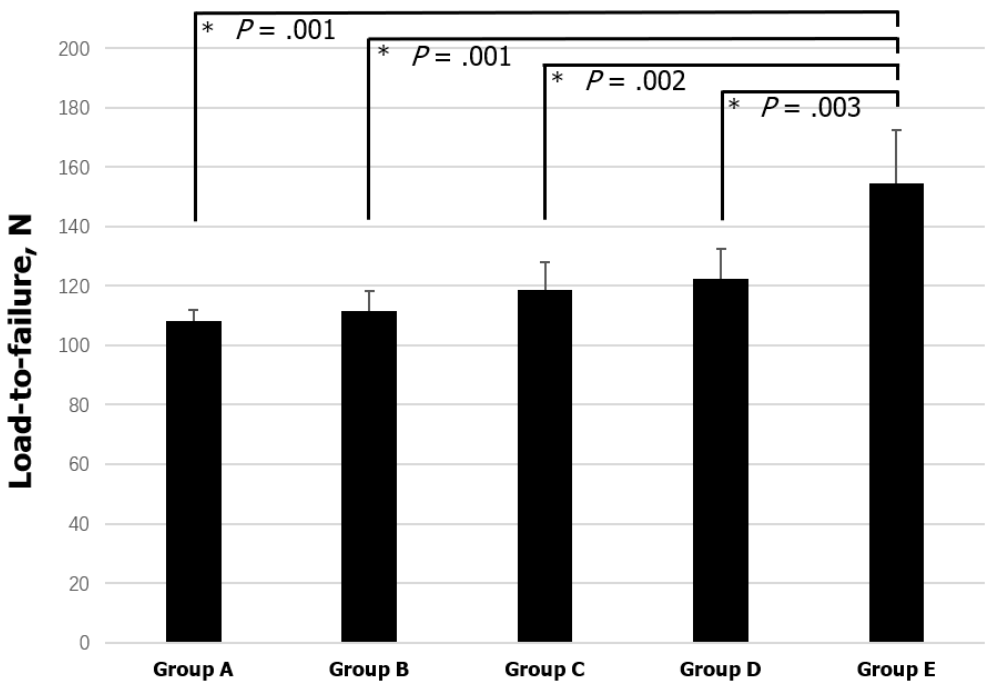

Table legend and tables

Table 1. Primer sequences for real-time polymerase chain reaction performed at 4 weeks and 12 weeks after repair

mRNA species	Forward	Reverse
COL1A1	5´-GGTCTTCTGCGACATGGACA-3´	5´-CCACACGTGCTTCTTCTCCT-3´
COL3A1	5´-GCTCTGCTTCATCCCACTGT-3´	5´-ATATTTGGCACGGTTCGGGT-3´
BMP-2	5´-GGGTGGAACGACTGGATTGT-3´	5´-TGCACGATGGCATGGTTAGT-3´
SCX	5´-ACAGATCTGCACCTTCTGCC-3´	5´-CCGTGACTCTTCAGTGGCAT-3´
SOX9	5´-GCCCAGAAGAGCCTCAAAGT-3´	5´-GGTACCAGTTGCCTTCAGCT-3´
ACAN	5´-GGATCTACCGCTGTGAGGTG-3´	5´-GTGGAGATGGCCCGATAGTG-3´
GAPDH	5´-GGAATCCACTGGCGTCTTCA-3´	5´-GGTTCACGCCCATCACAAAC-3´

COL1A1, collagen type I alpha 1; COL3A1, collagen type III alpha 1; BMP-2, bone morphogenetic protein 2; SCX, scleraxis; SOX9, SRY-box 9; ACAN, aggrecan; GAPDH, glyceraldehyde-3-phosphate dehydrogenase

Table 2. Quantitative real-time polymerase chain reaction analysis results in all groups at 4 weeks and 12 weeks after repair

	At 4 weeks after repair						At 12 weeks after repair					
	Group A (n = 7)	Group B (n = 6)	Group C (n = 7)	Group D (n = 6)	Group E (n = 6)	*P* value	Group A (n = 8)	Group B (n = 8)	Group C (n = 8)	Group D (n = 8)	Group E (n = 8)	*P* value
COL1A1	0.89 ± 0.06	0.92 ± 0.08	0.90 ± 0.06	0.92 ± 0.09	1.18 ± 0.08	**.008***	0.79 ± 0.12	0.83 ± 0.09	0.75 ± 0.22	0.92 ± 0.06	0.94 ± 0.06	.074
COL3A1	7.33 ± 0.59	8.26 ± 0.94	8.19 ± 0.75	8.39 ± 1.15	8.69 ± 0.47	.103	2.29 ± 0.96	2.02 ± 0.62	2.69 ± 0.97	2.63 ± 1.08	3.21 ± 1.50	.138
BMP-2	0.91 ± 0.09	0.97 ± 0.10	1.04 ± 0.19	1.03 ± 0.09	1.05 ± 0.09	.334	0.72 ± 0.19	0.62 ± 0.09	0.83 ± 0.38	0.67 ± 0.10	0.59 ± 0.13	.283
SCX	1.32 ± 0.10	1.33 ± 0.05	1.38 ± 0.29	1.38 ± 0.07	1.41 ± 0.08	.453	1.29 ± 0.38	1.28 ± 0.46	1.34 ± 0.33	1.28 ± 0.51	1.24 ± 0.45	.963
SOX9	1.14 ± 0.12	1.11 ± 0.10	1.12 ± 0.22	1.15 ± 0.07	1.22 ± 0.12	.665	0.69 ± 0.19	0.65 ± 0.08	0.65 ± 0.29	0.64 ± 0.12	0.68 ± 0.24	.975
ACAN	1.14 ± 0.20	1.13 ± 0.25	1.21 ± 0.22	1.14 ± 0.30	1.23 ± 0.25	.955	2.24 ± 0.62	1.91 ± 0.64	2.41 ± 0.52	2.56 ± 0.71	2.38 ± 0.48	.349

Group A, repair with normal saline injection; group B, repair with HA injection; group C, repair with three-dimensionally printed nanofiber sheet fixation; group D, repair with HA and rhPTH injection; group E, repair with three-dimensionally printed rhPTH-soaked nanofiber sheet fixation. Data are expressed as means ± SDs.

COL1A1, collagen type I alpha 1; COL3A1, collagen type III alpha 1; BMP-2, bone morphogenetic protein 2; SCX, scleraxis; SOX9, SRY-box 9; ACAN, aggrecan

The relative target gene expression ratio compared with glyceraldehyde 3-phosphate dehydrogenase (GAPDH) was quantified.

**Significantly different. There were significant differences in the expression level of COL1A1 between groups A and E (P = .001), groups B and E (P = .004), groups C and E (P = .001), and groups D and E (P = .004).*

Table 3. Histological grading[a] in all groups at 4 weeks and 12 weeks after repair

	At 4 weeks after repair									At 12 weeks after repair								
	Group A (n = 7)		Group B (n = 8)		Group C (n = 7)		Group D (n = 8)		P value	Group A (n = 8)		Group B (n = 8)		Group C (n = 8)		Group D (n = 8)		P value
Parameter	G0	G1	G2	G3	G0	G1	G2	G3	G0	G1	G2	G3	G0	G1	G2	G3	G0	G1	G2	G3	G0	G1	G2	G3	
Collagen fiber continuity	6	1	0	0	5	1	0	0	4	3	0	0	3	4	0	0	2	4	2	0	0	0	3	5	**0.001***
Collagen fiber orientation	5	2	0	0	4	2	0	0	5	2	0	0	3	4	0	0	2	4	2	0	0	1	4	3	0.559
Collagen fiber density	5	2	0	0	3	3	0	0	4	3	0	0	2	4	0	0	2	4	2	0	0	0	3	5	**0.001***
Maturation of the TTB junction	0	1	0	0	5	1	0	0	4	3	0	0	3	4	0	0	2	4	2	0	0	0	4	4	**0.003***

Group A, repair with normal saline injection; group B, repair with HA injection; group C, repair with three-dimensionally printed nanofiber sheet fixation; group D, repair with HA and rhPTH injection; group E, repair with three-dimensionally printed rhPTH-soaked nanofiber sheet fixation.

[a]Grading was as follows: grade 0, absent or minimal (0%–24%); grade 1, mild degree (25%–49%); grade 2, moderate degree (50%–74%); and grade 3, marked degree (75%–100%). Group A, repair with normal saline injection; group B, repair with HA injection; group C, repair with three-dimensionally printed nanofiber sheet fixation; group D, repair with HA and rhPTH injection; group E, repair with three-dimensionally printed rhPTH-soaked nanofiber sheet fixation. TTB, tendon-to-bone

[*]Significantly different. There were significant differences in the collagen fiber continuity between groups A and E ($P < .001$), groups B and E ($P = .001$), groups C and E ($P = .002$), and groups D and E ($P = .004$). There were significant differences in the collagen fiber density between groups A and E ($P < .001$), groups B and E ($P = .001$), groups C and E ($P = .002$), and groups D and E ($P = .002$). There were significant differences in the maturation of tendon-to-bone junction between groups A and E ($P = .001$), groups B and E ($P = .001$), groups C and E ($P = .002$), and groups D and E ($P = .004$).

Table 4. Biomechanical evaluation results in all groups at 12 weeks after repair

	Group A (n = 8)	Group B (n = 8)	Group C (n = 8)	Group D (n = 8)	Group E (n = 8)	*P* value
Load-to-failure, N	108.2 ± 3.6	111.6 ± 6.8	118.8 ± 9.1	122.4 ± 10.0	154.4 ± 18.0	**< 0.001***
Mode of tear (insertional: mid-substance tear), n	6:2	5:3	4:4	5:3	2:6	0.339

Group A, repair with normal saline injection; group B, repair with HA injection; group C, repair with three-dimensionally printed nanofiber sheet fixation; group D, repair with HA and rhPTH injection; group E, repair with three-dimensionally printed rhPTH-soaked nanofiber sheet fixation.

n, number; N, Newtons

**Significantly different. There were significant differences in the ultimate load-to-failure between groups A and E (P = .001), groups B and E (P = .001), groups C and E (P = .002), and groups D and E (P = .003).*

국문 초록

서론: 회전근 개 파열은 어깨 관절의 통증과 장애를 유발하는 진행성 질환으로 알려져 있다. 그러나 현재 수술 기법의 향상에도 불구하고 수술 후 회전근 개 봉합의 유합 실패는 11%에서 94% 사이의 실패율로 빈번한 합병증으로 남아 있다. 회전근 개 봉합 후 유합 실패에 있어서 골다공증은 하나의 독립적인 예후 인자이고, 또 재조합 인간 부갑상선 호르몬은 회전근개 파열이 있는 인간과 동물의 뼈 미네랄 밀도와 힘줄과 뼈의 유합을 촉진시킬 수 있다고 알려져 있다. 그러나 인간에 대해 재조합 인간 부갑상선 호르몬을 전신적, 반복적으로 주사함에 있어서 불편감 및 부작용을 유발할 수 있다. 본 연구에서는 만성 토끼 회전근 개 파열 모델에서 직접적, 국소적으로 재조합 인간 부갑상선 호르몬 주사 투여와 비교하여 3D 프린팅과 나노섬유를 이용한 재조합 인간 부갑상선 호르몬 담지 종이형 지지체가 회전근 개 봉합술 후 힘줄과 뼈의 유합에 미치는 영향에 대해 알아보고자 하였다.

재료 및 방법: 80마리의 토끼를 A, B, C, D, E 각 그룹당 16마리씩 무작위 배정하였다. 만성 회전근 개 파열 모델을 만들기 위해 전체 토끼의 양쪽 어깨에서 극상건을 절단하고 6주간 방치하였다. 극상건 절단 후 6주 뒤 다시 건 봉합술을 시행하고 봉합부위에: A그룹에서는 생리적 식염수를 주입하고, B그룹에서는 히알루론산를 주입하고, C그룹에서는 3D 프린팅과 나노섬유를 이용한 지지체를 고정하고, D그룹에서는 재조합 인간 부갑상선 호르몬 및 히알루론산을 혼합하여 주입하고, E그룹에서는 3D 프린팅과 나노섬유를 이용한 재조합 인간 부갑상선 호르몬 담지 종이형 지지체를 고정했다. 극상건 절단 후 6주 뒤 다시 건 봉합술을 시행하고 봉합부위에: A그룹에서는 생리적 식염수를 주입하고, B그룹에서는 히알루론산를

주입주입하고, C그룹에서는 3D 프린팅과 나노섬유를 이용한 지지체를 고정하고, D그룹에서는 재조합 인간 부갑상선 호르몬 및 히알루론산을 혼합하여 주입하고, E그룹에서는 3D 프린팅과 나노섬유를 이용한 재조합 인간 부갑상선 호르몬 담지 종이형 지지체를 고정했다. 결과 평가를 위해 유전학(mRNA 발현 평가) 및 조직학적 평가(건-골 이행부의 콜라겐 섬유의 연결성, 방향 및 밀집도, 건-골 이행부의 성숙도)를 건 봉합술 후 4주에 각 그룹의 절반 마리수의 토끼에 대하여 시행하였다. 마찬가지로 건 봉합술 후 12주에도 유전학 및 조직학적 평가를 시행하였고, 추가적으로 생역학적 평가(파열 부위, 최대 파열 강도)를 각 그룹의 나머지 토끼에 대하여 시행하였다.

결과: 회전근 개 건의 유전학적 평가 결과, 극상건 봉합술 후 4주 때 E그룹에서 A, B, C, D 네개 그룹에 비해 collagen type I alpha 1의 mRNA발현이 유의하게 높았는데(P = .008), 봉합술 후 12주 때에는 4주 때 보다 collagen type I alpha 1의 발현 수준이 전체 그룹에서 하향된 양상을 보였고 통계학적으로 유의하진 않았다. 극상건-골 결합의 조직학적 검사 결과, 극상건 봉합술 후 12주 때 E그룹에서 기타 4개 대조군 그룹에 비해 건-골 결합부의 콜라겐 섬유 연결성, 밀집도, 성숙도가 더 높은 양상을 확인할 수 있었다(각각 P = .001, P = .001 및 P = .003). 생역학적 검사에서도 유사한 양상을 보였는데, 극상건 봉합술 후 12주 때 E그룹은 기타 4개 대조군 그룹에 비해 파열 강도가 유의하게 높았다(P < .001).

결론: 3D 프린팅과 나노섬유를 이용한 재조합 인간 부갑상선 호르몬 담지 종이형 지지체는 만성 토끼 회전근 개 파열 모델에서 봉합술 후 건-골 결합 치유를 촉진시킨다.

색인 단어: 재조합 인간 부갑상선 호르몬; 3D 프린팅; 나노섬유 지지체;

건-골 결합 치유; 만성 회전근개 파열; 토끼 모델

학번: 2020-37085